ACSNANO
www.acsnano.org
ARTICLE

Tailoring MoS_2 Exciton–Plasmon Interaction by Optical Spin–Orbit Coupling

Ziwei Li,[†,§] Yu Li,[†,§] Tianyang Han,[†] Xingli Wang,[‡] Ying Yu,[†] Bengkang Tay,[‡] Zheng Liu,[‡] and Zheyu Fang*[,†]

[†]School of Physics, State Key Lab for Mesoscopic Physics; Academy for Advanced Interdisciplinary Studies; Collaborative Innovation Center of Quantum Matter, Peking University, Beijing 100871, China

[‡]NOVITAS, School of Electrical and Electronic Engineering, Nanyang Technology University, Singapore 639798

Supporting Information

ABSTRACT: **Molybdenum disulfide (MoS_2) monolayer as one of the atomic thickness two-dimensional materials has remarkable electronic and optical properties, which is an ideal candidate for a wide range of optoelectronic applications. However, the atomic monolayer thickness poses a significant challenge in MoS_2 photoluminescence emission due to weak light–matter interaction. Here, we investigate the MoS_2 exciton–plasmon interaction with spin–orbit coupling of light. The plasmonic spiral rings with subwavelength dimensions are designed and fabricated on hybrid substrates. MoS_2 photoluminescence enhancement can be actively controlled by changing the incident optical spin states, laser powers, and the nanospiral geometries, which is arising from the change of field enhancement at near-field region. Planar light-emitting devices based on spin–orbit coupling (SOC) effect were further realized and flexibly controlled by changing the polarization of light. The SOC effect is discussed by the accumulation of geometric and dynamic phases, which can be demonstrated and elaborated by the Majorana sphere model. Our results provide a way to manipulate MoS_2 light–matter interaction actively and can be further applied in the spin-dependent light-emitting devices at the nanoscale.**

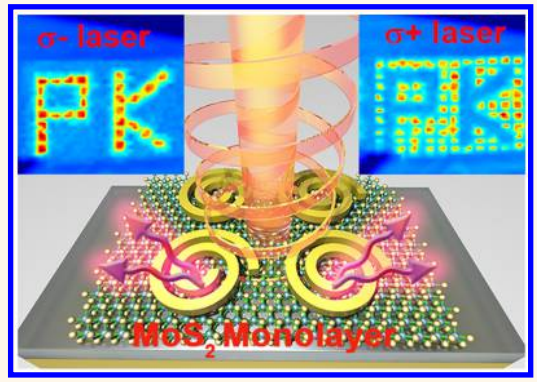

KEYWORDS: *MoS_2, photoluminescence, exciton–plasmon interaction, spin–orbit coupling*

The MoS_2 monolayer is a promising two-dimensional (2D) semiconductor with direct band gap electronic structure, notable flexibility, and tunable optical emission, which has great potential for the application of optoelectronic devices.[1−3] Valence band splitting induced by strong spin–orbit coupling (SOC) results in multiexciton photoluminescence (PL), and the extraordinary exciton binding energy is utilized to generate exciton emission at the room temperature.[4] With these properties, it has motivated extensive interest for researchers to explore its potential physical phenomena, especially on light–matter interaction, such as multiexciton PL, interlayer exciton coupling, and valley polarization effect.[5−7] However, enhancing and modulating the PL emission of MoS_2 monolayer are still a great challenge for its practical applications.

Great efforts have been devoted to realize the active control of MoS_2 PL by utilizing photonic cavity modes and metallic surface plasmons. Photonic microcavities formed by low-loss dielectric material are ideal structures for pumping exciton lasing.[8,9] Localized field enhancement induced by plasmonic "bowtie" and "dimer" structures is an alternative way for enhancing MoS_2 PL emissions.[10−13] Nanowire-coupled exciton emission is remarkable with high coupling efficiency, and selective amplification of MoS_2 PL based on exciton–plasmon interaction is realized experimentally.[14−17] However, most designed structures must be fabricated precisely with the structure geometries and the coupling distance, which limits the development of active-controlled optoelectronic devices in the future.

The SOC of light is the interaction between spin angular momentum (SAM), intrinsic and extrinsic orbital angular momentum (OAM),[18,19] involving SAM to intrinsic OAM conversion in nanoparticles,[20,21] SAM to extrinsic OAM conversion in directional surface plasmon propagation,[22,23] and intrinsic OAM to extrinsic OAM conversion in other systems.[24,25] SOC effect can be generated when plasmonic spiral rings coupled with circular polarized light perform the spin-dependent optical phenomena. It has been widely reported that surface plasmon polaritons (SPPs) propagation in the near-field can be modulated by the geometric and dynamic

Received: October 10, 2016
Accepted: December 2, 2016
Published: December 2, 2016

DOI: 10.1021/acsnano.6b06834
ACS Nano 2017, 11, 1165–1171

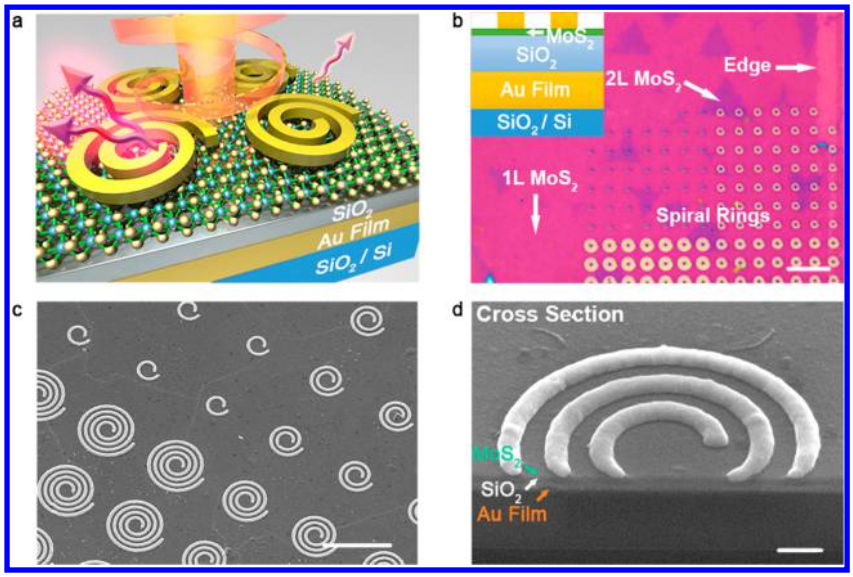

Figure 1. Schematic of MDM structure and its characteristic properties. (a) Schematic of spiral ring structure on SiO_2/Au/SiO_2/Si substrate with circular polarized light excitation. PL intensity was enhanced when MoS_2 monolayer coupled with spiral rings. (b) The optical image of MoS_2 film and spiral ring arrays; scale bar is 5 μm. Inset shows the schematic cross-section view of MDM structure. (c) The SEM image of spiral ring arrays with variant ring numbers ranging from 1 to 4; scale bar is 2.5 μm. (d) Cross section view of 3-turn spiral ring at a tilted angle 52°; scale bar is 200 nm.

phase, such as plasmonic vortex,[26,27] and plasmonic lens focusing.[28,29] Manipulating the SOC of light with plasmonic structures provides an additional method for tailoring the light−matter interaction in nanophotonics.[30−32]

In this article, we use metal-dielectric-metal (MDM) plasmonic structures to investigate the MoS_2 exciton−plasmon interaction by spectroscopic measurements and numerical simulations. MoS_2 excitons coupled with SPPs wave can enhance the MoS_2 PL more than 10 times. Moreover, the MoS_2 PL intensity can be further manipulated by tailoring the SOC effect, which can be controlled by the optical spin states, spiral geometries, and the incident laser powers. The SOC-dependent electric-field (E-field) distribution provides direct evidence for actively controlled SPPs focusing. The amplification of MoS_2 PL tends to be saturated at intense laser powers, which is due to the competition of exciton generation rate and recombination rate. A theoretical model of phase accumulation is proposed to understand the mechanism, involving SOC-induced geometric phase and spiral-pitch-induced dynamic phase. Tailoring the SOC effect in nanospiral ring offers a way for potential applications on MoS_2 light-emitting device. This interaction between MoS_2 exciton and SPPs can be exploited in the development of a class of spin-dependent nanophotonic devices.

RESULTS AND DISCUSSION

Device Fabrication and Spectral Characterization. Figure 1a is the schematic of the MDM structure with spiral rings and MoS_2 monolayer under circular polarized light excitation. Compared with pure MoS_2 film on the same hybrid substrate, the PL emission is enhanced when the MoS_2 monolayer couples with spiral structures. The MoS_2 monolayer was grown by chemical vapor deposition (CVD) method and then transferred onto 35 nm SiO_2 with 30 nm golden mirror layer. Spiral rings were patterned by E-beam lithography and deposited with 40 nm Au film. Figure 1b presents the optical image of spiral ring arrays on the hybrid structure. Observed from the color contrast at the film edge, most of the area is the monolayer region, and few two-layered MoS_2 flakes appear as the dark purple. The monolayer property of the sample can be verified by the PL mapping and the energy difference of E^1_{2g} and A_{1g}.[33] Raman signals were dramatically enhanced on this MDM structure, which is arising from the surface plasmon enhanced Raman scattering (see Supporting Information Figure S1).[34,35] Inset shows the schematic cross-section view of the MDM structure, where the green layer represents the MoS_2 monolayer. In Figure 1c, SEM image shows the morphology of spiral ring arrays on the MoS_2 monolayer with variant ring numbers ranging from 1 to 4. Figure 1d shows the cross-section view of 3-turn spiral ring at a tilted angle 52°, where the layer properties can be observed by the color contrast obviously.

Active-Controlled PL Enhancement. Figure 2 shows the difference of PL intensity of pure MoS_2 monolayer and MoS_2 interacting with spiral rings. Inset shows the SEM image of measured 2-turn spiral ring structure at a tilted view. The

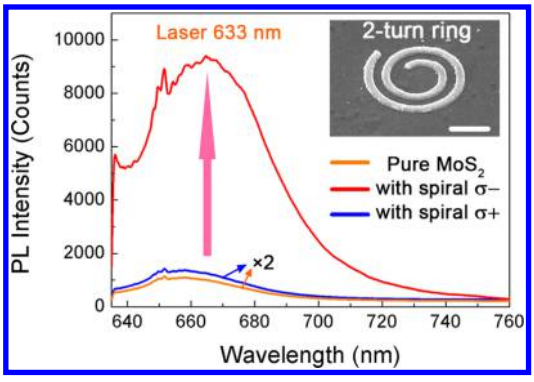

Figure 2. PL spectra of MoS_2 monolayer with and without spiral structures, under the excitation of different circular polarized light at 633 nm. Laser power was controlled at 2.1 mW. Inset shows the cross section view of 2-turn spiral ring; scale bar is 400 nm.

DOI: 10.1021/acsnano.6b06834
ACS Nano 2017, 11, 1165−1171

Purcell enhancement factor can be defined as $\varepsilon = I_{wi}/I_{wo}$, where I_{wi} (I_{wo}) is the maximum intensity of MoS_2 with (without) nanospiral rings. Under the excitation of left-hand circular polarized light (LCP, red), the maximum of PL enhancement of MoS_2 monolayer is about 10 times higher than the pure MoS_2 (orange), which means ε is larger than 10. However, PL signals are barely enhanced with the illumination of right-hand circular polarized light (RCP, blue), and ε is nearly 1. This spectroscopic change can be actively controlled by the polarization of the incident light, which provides an efficient way for tailoring the exciton−plasmon interaction.

The Purcell enhancement ε is associated with systematic collection efficiency, quantum efficiency, and E-field enhancement.[36] The collection and quantum efficiency are analyzed in detail, and spin-dependent E-field enhancement induced by nanospiral rings mainly gives rise to the huge difference in ε (see Figure S2). The near-field intensity and phase distributions are simulated under LCP and RCP excitation to understand the mechanism of the PL enhancement. Figure 3a shows the SEM image of 2-turn spiral rings, and their structural parameters are shown in Figure 3b. The start radius of the spiral cavity is designed to be 150 nm. The grating width and the spiral pitch are 100 and 200 nm, respectively. These structural parameters are chosen to fabricate the spiral structures because the strong field enhancement can be generated at the ring center, and structural diameters are smaller than the laser beam (See Figure S3). The spiral rings couple LCP incident light at the wavelength of 633 nm, which can generate SPPs with the wavelength (λ_{SPP}) about 400 nm (see Figure S4).

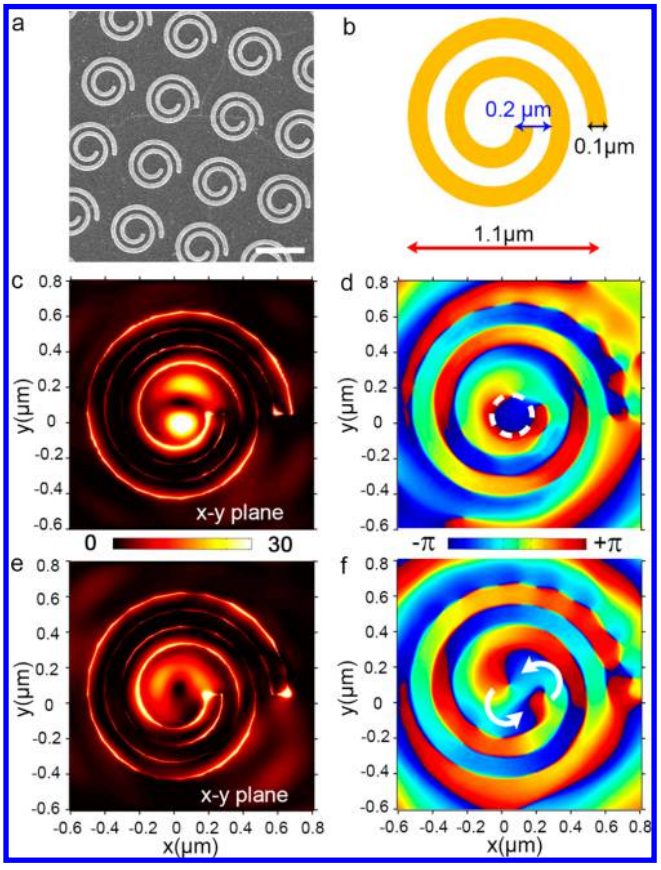

Figure 3. Geometric structure and spin-dependent E-field distribution of 2-turn spiral ring. (a) SEM image of 2-turn spiral rings; scale bar is 1 μm. (b) The grating width, the spiral pitch, and the diameter of outer contour are 0.1, 0.2, and 1.1 μm, respectively. (c) Near-field intensity of $|E_z|^2$ at $x-y$ plane with a focusing spot under LCP excitation. (c) Phase map of E_z at $x-y$ plane for LCP excitation. (e) Near-field intensity of $|E_z|^2$ at $x-y$ plane without focusing under RCP excitation. (f) Phase map of E_z at $x-y$ plane for RCP excitation.

Figure 3c shows the near-field intensity at $x-y$ plane for LCP excitation. When spiral ring interacts with LCP light, SPPs are generated by a space-variant structure, coherent and propagate toward to the ring center forming a focusing spot. Figure 3d shows the corresponding phase map of 2-turn spiral ring at $x-y$ plane with LCP excitation. The phase at the center of the spiral ring shows locally uniform distribution with $-\pi$ as the dotted circle noted in Figure 3d, which is arising from the conversion of spin AM to OAM. The obvious PL enhancement under LCP excitation is because of the interaction of exciton and SPPs field. Figure 3e is the distribution of RCP-induced weak E-field without focusing spot. At the center, phase changes from π to $-\pi$ for two-round anticlockwise as shown in Figure 3f. SPPs propagate as usual with RCP excitation, but their phase cannot compensate generating a local uniformed spot with $-\pi$, which results in nonfocusing mode. Therefore, the PL intensity shows little enhancement with RCP excitation due to the poor coupling process. The phase change is arising from the conversion of spin AM and intrinsic OAM. The location of focusing spot is related with the conversion of spin AM and extrinsic OAM in our spatially varying structures.

Furthermore, tailoring MoS_2 exciton−plasmon interaction by SOC effect can be applied in 2D light-emitting device (see Figure S5). The 2-turn nanospiral is a kind of chiral structure with different spiral orientations, which shows a distinctive response when interacting with a certain circular polarized light. Under LCP excitation, MoS_2 coupled with nanospirals in a specific spiral orientation emits bright PL showing a convex "PK" pattern. However, a concave "PK" pattern can be observed under RCP illumination. By tailoring the SOC effect in our MDM spiral structures, the 2D light-emitting device involving exciton−plasmon interaction can be actively controlled by optical polarization, which holds great potential for the development of light-emitting applications based on 2D materials in the future.

Laser-Power-Dependent Coupling. The exciton−plasmon interaction is associated with laser powers, and PL intensities of MoS_2 coupled with and without spiral rings were investigated in details (see Figure S6). When MoS_2 coupled with a 2-turn spiral ring under 633 nm laser excitation, PL intensity increases dramatically as laser power increases from 0.35 to 5.6 mW, but peak energy shows nonshifting (dotted line) as shown in Figure 4a. Figure 4b shows the plots of log−log scale PL intensity with (blue circle) and without (red circle) SOC effect. The relationship between total PL intensity (I) and laser power can be approximately written as $I = (P)^m$, where m denotes exponent. For MoS_2 without a spiral ring, m is fitted to be 0.86 with laser powers ranging from 0.17 to 5.6 mW. When MoS_2 couples with SPPs focusing, m is as same as 0.86 at low powers ($P < 2.1$ mW). However, for $P > 2.1$ mW, m is degraded to 0.65 as the exciton radiation starts to be saturated. The enhancement factor ε increases first at a lower power and then decreases when the power becomes larger, and the maximum of factor ε can reach more than 10 at 0.21 mW. This enhancement can be understood and verified by theoretical calculations, where the factor ε in our structure can be estimated as 13.5 (see Figure S2).

DOI: 10.1021/acsnano.6b06834
ACS Nano 2017, 11, 1165−1171

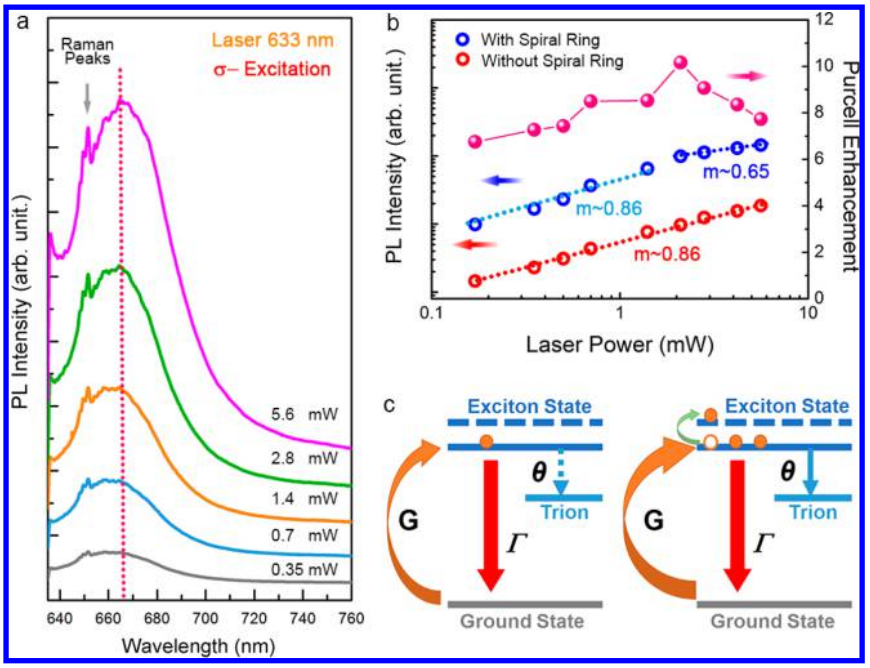

Figure 4. Analysis of PL change and schematic of a three-energy-level model. (a) PL spectra change with the increasing laser powers. (b) Plots of PL intensity with (blue) and without (red) SOC coupling and corresponding Purcell enhancement (pink balls) under different laser powers. (c) Schematic view of the three-energy-level model and competition of exciton generation rate and recombination rate.

Under LCP excitation, the hot carriers induced from absorption are excited, cooling down to the lowest exciton energy, and finally recombine *via* radiative or nonradiative decay. Meanwhile, SPPs are generated, couple with MoS_2 exciton, and propagate toward the center of spiral structure to realize the plasmonic focusing. Figure 4c shows the schematic of a three-energy-level model, involving exciton, trion, and ground state. The generated exciton recombines in a radiative process and also transforms into trion during a nonradiative decay. The exciton rate equation of steady-state is $N = G/(\Gamma + \theta)$, where G, Γ, and θ are the exciton generation rate, the exciton recombination rate, and the trion formation rate, respectively. Under weak light excitation, there is not enough exciton to fill the exciton state, and Γ is directly related with G because θ is negligible in this situation. When the laser power is increased, the strong field strengthens the charge−charge interaction and pumps the exciton into higher unoccupied exciton states. Besides, θ also increases, which may create more charge exciton (trion, biexciton) in a nonradiative decay. The competition of exciton generation rate and recombination rate gives rise to the change of Purcell enhancement and exponential dependence with the increased laser powers.[16]

Ring-Number-Dependent Coupling. The E-field and phase distribution is also related with the ring number of nanospirals (see Figure S7), and the influence of exciton−plasmon interaction on the ring number is further investigated. All of the simulations and experiments were carried out under LCP illumination with the incident wavelength of 633 nm. Figure 5a shows SEM images of 1-, 2-, 3- and 4-turn spiral rings on the hybrid structure. The grating width and the spiral pitch are controlled at 100 and 200 nm, respectively. The corresponding E-field intensities are shown in Figure 5b, where we can see that the focusing effect happens in the nanospiral rings with an even number turn, which can be explained by two effects: including phase compensation induced by outer gratings and the inner grating coupling at subwavelength dimensions. The phase distribution exhibits a strong dependence on the ring number as shown in Figure 5c. For odd number spiral rings, the phase changes from $-\pi$ to π for one-round anticlockwise, however, it appears as a local uniformed spot with $-\pi$ in even number spiral rings. The focusing and nonfocusing phenomena in different rings can be optimized and selected for PL enhancement. This ring-number-dependent focusing phenomena can be observed from PL mapping images in Figure 5d. The layer properties can be clearly verified by the color contrast, where most of the "green" area is MoS_2 monolayer film, and few two-layered MoS_2 flakes show dark blue in the shape of triangle. As predicted, PL intensity is dramatically enhanced when the MoS_2 monolayer couples with 2- and 4-turn spiral rings. However, the intensity enhancement almost disappears in the 1- and 3-turn spiral rings.

Spin−Orbital Coupling Effect. The SOC phenomena can be interpreted by a Majorana sphere model[29,37] as shown in Figure 6a, including spin states ($\sigma_\pm$), dynamic phase (Φ_d), and geometric Berry phase (Φ_g). The LCP (RCP) light can be represented as a spin state as $|\sigma_- \geq -1$ ($|\sigma_+ \geq +1$), which can be shown by two unit vector **u** and **v**. A geodesic arc connecting the north and south poles represents the evolution of light from circular polarized light to SPP wave. The area surrounded by geodesic arc *I* and *II* on the Majorana sphere is the geometric Berry phase $\Phi_g = -(\Omega_v + \Omega_u)/2$ (pink surface), which intersects the $x-y$ plane at angle φ. The general case can be given by $\Phi_g = -\sigma_\pm\varphi$. Moreover, the dynamic phase Φ_d arises as a result of a space-variant path difference induced by the gratings spiral pitch, which can be described by $p{\cdot}p$ is defined as L_{pitch}/λ_{SPP}, where L_{pitch} is the length of the spiral pitch. More detailed descriptions on basic Majorana sphere can be found in Figure S8. Figure 6b shows the difference of dynamic phase in spiral rings with $p = 1$ and $p = 1/2$. The structure parameters of spiral ring are $r = r_0 + \varphi{\cdot}\lambda_{SPP}/2\pi$ with $p = 1$. When grating

DOI: 10.1021/acsnano.6b06834
ACS Nano 2017, 11, 1165−1171

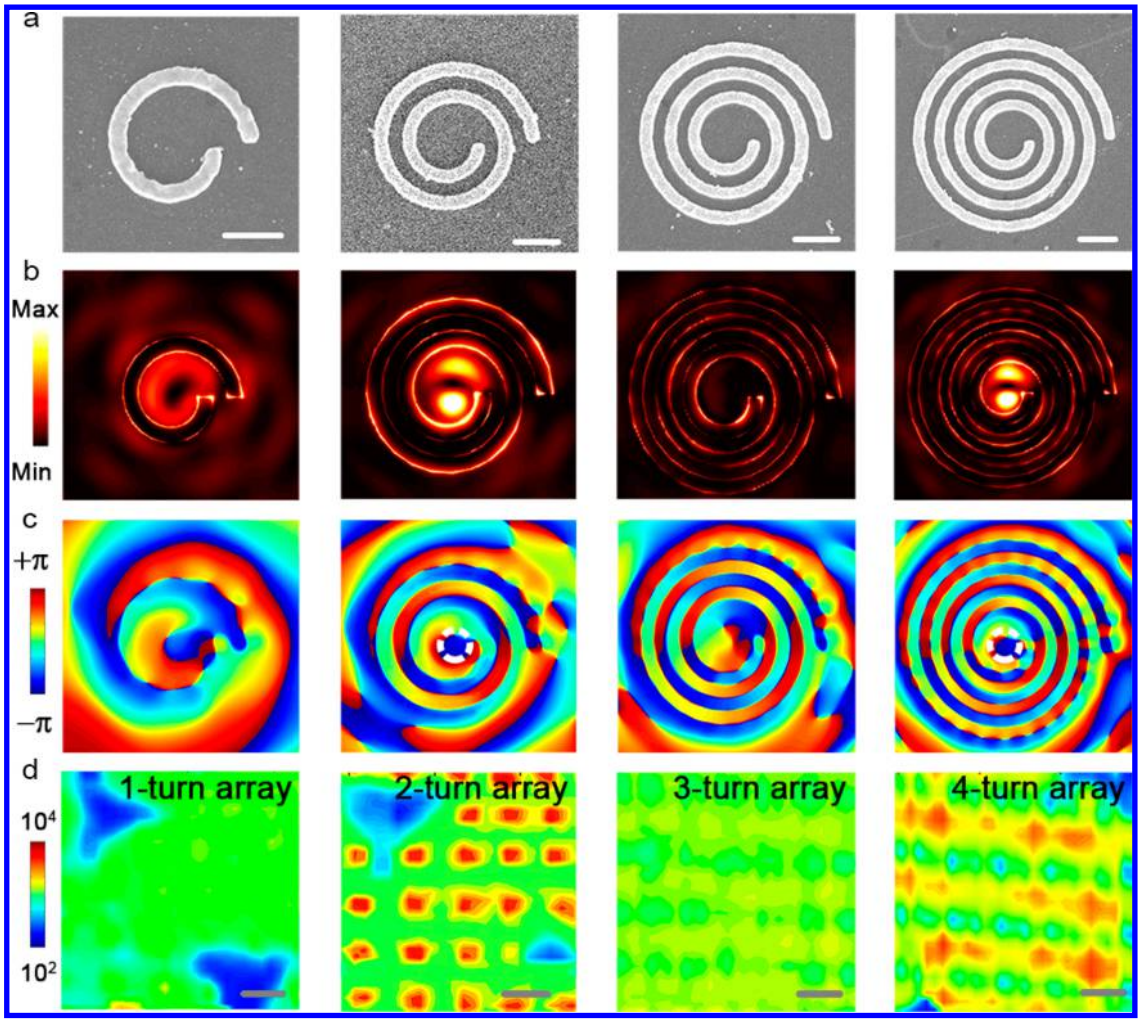

Figure 5. SOC-dependent phenomena with various ring number of spiral structures. (a) SEM images of 1-, 2-, 3-, and 4-turn spiral rings; scale bar is 400 nm. (b) Corresponding E-electric intensity with LCP excitation at 633 nm. Focusing field can be obtained from 2- and 4-turn spiral rings. (c) Corresponding phase distribution for 1-, 2-, 3-, 4-turn spiral rings. (d) PL mapping of MoS_2 patterned with spiral ring arrays; scale bar is 3 μm.

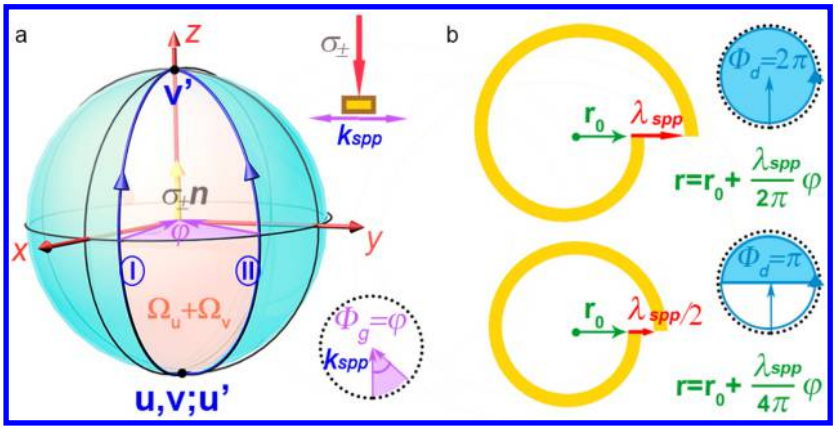

Figure 6. (a) Schematic view of phase accumulation in Majorana sphere model, including spin states and geometric Berry phase. (b) Dynamic phase in different nanospiral rings with gratings rotating for 2π geometrically.

rotates 2π geometrically, both Φ_g and Φ_d are 2π. In this situation, plasmonic focusing is independent of the number of spiral rings because the total phase $\Phi = \Phi_g + \Phi_d$ is 4π.[29] The total topological charge of the plasmonic vortex is $l = -(\sigma_\pm + p)$. However, the parameters of spiral ring are $r = r_0 + \varphi \cdot \lambda_{SPP}/4\pi$ with $p = 1/2$. When the grating rotates 2π geometrically, the Φ_g and Φ_d are 2π and π, respectively. The total phase $\Phi = \Phi_g + \Phi_d$ is 3π, which means an incomplete phase compensation. The selective rule fails because the topological charge must be an integer. All the above discussions are based on a general case, where SPPs propagation and coherent happen on a metallic film beyond subwavelength dimensions. Specifically, our

DOI: 10.1021/acsnano.6b06834
ACS Nano 2017, 11, 1165−1171

designed hybrid structures are plasmonic spirals with $p = 1/2$ at subwavelength dimensions, which emergent properties are manifest in complex intraparticle interactions. The E-field phase and focusing modes are mainly arising from SPPs interference and may also be influenced by inner grating coupling in the near-field.

CONCLUSIONS

In summary, we have demonstrated that tailoring the SOC effect opens up a strategy for active control of MoS_2 exciton−plasmon interaction. The mechanism is that the SPP focusing field amplifies the exciton emission of MoS_2 monolayer, which is induced by the interaction of MoS_2 exciton and plasmon. The emission signals are dramatically enhanced and reversibly controlled by changing optical spin states, laser powers, and spiral structure parameters. PL efficiency of MoS_2 monolayer is easily saturated with plasmon coupling due to the competition of exciton generation and recombination rate. In this hybrid structure, the significant role of tailoring SOC effect in exciton−plasmon interaction is identified and elaborated by the Majorana sphere model. 2D light-emitting devices based on plasmon−exciton interaction were realized and can be actively controlled by circular polarized lights. Our work provides a potential opportunity for the exploration of light−matter interaction in the nanoscale and promotes the development of spin-dependent nanophotonic devices.

MATERIALS AND METHODS

Preparation of MoS_2 Monolayers. MoS_2 samples were synthesized by CVD. Sulfur (S) and molybdenum oxide (MoO_3) powder are the source of S and Mo, respectively. A boat with MoO_3 powder was put into a fused quartz tube located at the center of the CVD furnace. A piece of SiO_2/Si wafer was suspended on the boat. The furnace temperature was raised up to 750 °C in 15 min and was held for 20 min, yielding MoS_2 triangle domains. During the process, 50 sccm of argon was used as the carrier gas, and the growth was carried out under atmospheric pressure. Samples with spin-coated PMMA can be transferred onto prepared substrates by wetting transfer methods.

Fabrication of Spiral Rings. Spiral ring structures were fabricated by E-beam lithography. A drop of PMMA A2 was spin-coated on the prepared substrate at 3000 rpm for 50 s and then heated on a hot plate for 5 min. The designed structure was drawn by nanometer pattern generation system (NPGS) and patterned by FEI Helios600i scanning electron microscope (SEM). A 40 nm Au film was evaporated by E-beam evaporation system and then lifted off after soaking in acetone for 2 h.

Simulations and Optical Measurements. Simulations on electromagnetic field were performed by finite-difference time-domain (FDTD) solutions, and the experimental spectra were measured by a home-built spectra system. An iHR550 Raman spectrometer from Horiba was utilized with 1200 g mm^{-1} and 2400 g mm^{-1} gratings. The Raman spectra was detected using 2400 g mm^{-1} gratings for high resolution. PL spectra and mapping were measured with 1200 g mm^{-1}. The objective lens is 50× magnification. The excitation laser is 633 nm He−Ne laser, which was focused to a diffraction-limited spot about 2 μm. For PL mapping measurements, the laser power was controlled at 1.4 mW, and the PL intensity ranging from 645 to 685 nm was integrated to draw the mapping images.

ASSOCIATED CONTENT

Supporting Information

The Supporting Information is available free of charge on the ACS Publications website at DOI: 10.1021/acsnano.6b06834.

Figures S1: Optical properties of MoS_2; S2: Purcell enhancement; S3: E-field distribution at $x-z$ plane; S4: Wavelength of SPPs; S5: Light-emitting device; S6: PL spectra changing with laser powers; S7: Electric phase and field distribution; S8: SOC in Majorana sphere; and S9: SEM images (PDF)

AUTHOR INFORMATION

Corresponding Author

*E-mail: zhyfang@pku.edu.cn.

ORCID

Ziwei Li: 0000-0002-2987-7186

Zheyu Fang: 0000-0001-5780-0728

Author Contributions

§These authors contributed equally to this work.

Notes

The authors declare no competing financial interest.

ACKNOWLEDGMENTS

This work is supported by National Basic Research Program of China (973 Program, grant no. 2015CB932403), National Science Foundation of China (grant nos. 61422501, 11674012, 11374023, and 61521004), Beijing Natural Science Foundation (grant no. L140007), and Foundation for the Author of National Excellent Doctoral Dissertation of PR China (grant no. 201420), National Program for Support of Top-notch Young Professionals. This work is also supported by the Singapore National Research Foundation under NRF-RF award no. NRF-RF2013-08. B.K.T. and X.W. gratefully acknowledge funding support from NTU-A*STAR Silicon Technologies Centre of Excellence (grant no. 11235100003).

REFERENCES

(1) Mak, K. F.; Lee, C.; Hone, J.; Shan, J.; Heinz, T. F. Atomically Thin MoS_2: A New Direct-Gap Semiconductor. *Phys. Rev. Lett.* **2010**, *105*, 474−479.

(2) Conley, H. J.; Wang, B.; Ziegler, J. I.; Haglund, R. F.; Pantelides, S. T.; Bolotin, K. I. Bandgap Engineering of Strained Monolayer and Bilayer MoS_2. *Nano Lett.* **2013**, *13*, 3626−3630.

(3) Ross, J. S.; Wu, S.; Yu, H.; Ghimire, N. J.; Jones, A. M.; Aivazian, G.; Yan, J.; Mandrus, D. G.; Xiao, D.; Yao, W.; Xu, X. Electric Control of Neutral and Charged Excitons in a Monolayer Semiconductor. *Nat. Commun.* **2013**, *4*, 1474.

(4) Mak, K. F.; He, K.; Lee, C.; Lee, G. H.; Hone, J.; Heinz, T. F.; Jie, S. Tightly Bound Trions in Monolayer MoS_2. *Nat. Mater.* **2012**, *12*, 207−211.

(5) Kang, Y.; Najmaei, S.; Liu, Z.; Bao, Y.; Wang, Y.; Zhu, X.; Halas, N. J.; Nordlander, P.; Ajayan, P. M.; Lou, J.; Fang, Z. Plasmonic Hot Electron Induced Structural Phase Transition in a MoS_2 Monolayer. *Adv. Mater.* **2014**, *26*, 6467−6471.

(6) Zhan, Y.; Liu, Z.; Najmaei, S.; Ajayan, P. M.; Lou, J. Large Area Vapor Phase Growth and Characterization of MoS_2 Atomic Layers on SiO_2 Substrate. *Small* **2012**, *8*, 966−971.

(7) Li, Z.; Ye, R.; Feng, R.; Kang, Y.; Zhu, X.; Tour, J. M.; Fang, Z. Graphene Quantum Dots Doping of MoS_2 Monolayers. *Adv. Mater.* **2015**, *27*, 5235−5240.

(8) Yang, W.; Shang, J.; Wang, J.; Shen, X.; Cao, B.; Peimyoo, N.; Zou, C.; Chen, Y.; Wang, Y.; Cong, C.; Huang, W.; Yu, T. Electrically Tunable Valley-Light Emitting Diode (VLED) Based on CVD-Grown Monolayer WS_2. *Nano Lett.* **2016**, *16*, 1560−1567.

(9) Wu, S.; Buckley, S.; Schaibley, J. R.; Feng, L.; Yan, J.; Mandrus, D. G.; Hatami, F.; Yao, W.; Vučković, J.; Majumdar, A.; Xu, X. Monolayer Semiconductor Nanocavity Lasers with Ultralow Thresholds. *Nature* **2015**, *520*, 69−72.

DOI: 10.1021/acsnano.6b06834
ACS Nano 2017, 11, 1165−1171

(10) Liu, X.; Galfsky, T.; Sun, Z.; Xia, F.; Lin, E. C.; Lee, Y. H.; Kéna-Cohen, S.; Menon, V. M. Strong Light-Matter Coupling in Two-Dimensional Atomic Crystals. *Nat. Photonics* **2014**, *9*, 30−34.
(11) Butun, S.; Tongay, S.; Aydin, K. Enhanced Light Emission from Large-Area Monolayer MoS_2 Using Plasmonic Nanodisc Arrays. *Nano Lett.* **2015**, *15*, 2700−2704.
(12) Lee, B.; Park, J.; Han, G. H.; Ee, H. S.; Naylor, C. H.; Liu, W.; Johnson, A. T. C.; Agarwal, R. Fano Resonance and Spectrally Modified Photoluminescence Enhancement in Monolayer MoS_2 Integrated with Plasmonic Nanoantenna Array. *Nano Lett.* **2015**, *15*, 3646−3653.
(13) Yang, A.; Li, Z.; Knudson, M. P.; Hryn, A. J.; Wang, W.; Aydin, K.; Odom, T. W. Unidirectional Lasing from Template-Stripped Two-Dimensional Plasmonic Crystals. *ACS Nano* **2015**, *9*, 11582−11588.
(14) Li, Z.; Xiao, Y.; Gong, Y.; Wang, Z.; Kang, Y.; Zu, S.; Ajayan, P. M.; Nordlander, P.; Fang, Z. Active Light Control of the MoS_2 Monolayer Exciton Binding Energy. *ACS Nano* **2015**, *9*, 10158−10164.
(15) Fedutik, Y.; Temnov, V. V.; Schöps, O.; Woggon, U.; Artemyev, M. V. Exciton-Plasmon-Photon Conversion in Plasmonic Nanostructures. *Phys. Rev. Lett.* **2007**, *99*, 136802.
(16) Lee, H. S.; Kim, M. S.; Jin, Y.; Han, G. H.; Lee, Y. H.; Kim, J. Selective Amplification of the Primary Exciton in A MoS_2 Monolayer. *Phys. Rev. Lett.* **2015**, *115*, 226801.
(17) de Torres, J.; Ferrand, P.; Colas des Francs, G.; Wenger, J. Coupling Emitters and Silver Nanowires to Achieve Long-Range Plasmon-Mediated Fluorescence Energy Transfer. *ACS Nano* **2016**, *10*, 3968−3976.
(18) Bliokh, K. Y.; Niv, A.; Kleiner, V.; Hasman, E. Geometrodynamics of Spinning Light. *Nat. Photonics* **2008**, *2*, 748−753.
(19) Bliokh, K. Y.; Rodríguez-Fortuño, F. J.; Nori, F.; Zayats, A. V. Spin-Orbit Interactions of Light. *Nat. Photonics* **2015**, *9*, 796−808.
(20) O'Connor, D.; Ginzburg, P.; Rodríguez-Fortuño, F. J.; Wurtz, G. A.; Zayats, A. V. Spin−Orbit Coupling in Surface Plasmon Scattering by Nanostructures. *Nat. Commun.* **2014**, *5*, 5327.
(21) Dogariu, A.; Schwartz, C. Conservation of Angular Momentum of Light in Single Scattering. *Opt. Express* **2006**, *14*, 8425−8433.
(22) Li, L.; Li, T.; Wang, S.; Zhu, S.; Zhang, X. Broad Band Focusing and Demultiplexing of In-Plane Propagating Surface Plasmons. *Nano Lett.* **2011**, *11*, 4357−4361.
(23) Rodríguez-Fortuño, F. J.; Marino, G.; Ginzburg, P.; O'Connor, D.; Martínez, A.; Wurtz, G. A.; Zayats, A. V. Near-Field Interference for the Unidirectional Excitation of Electromagnetic Guided Modes. *Science* **2013**, *340*, 328−330.
(24) Bliokh, K. Y. Geometrical Optics of Beams with Vortices: Berry Phase and Orbital Angular Momentum Hall Effect. *Phys. Rev. Lett.* **2006**, *97*, 043901.
(25) Bialynicki-Birula, I.; Bialynicka-Birula, Z. Berry's Phase in the Relativistic Theory of Spinning Particles. *Phys. Rev. D: Part. Fields* **1987**, *35*, 2383−2387.
(26) Kim, H.; Park, J.; Cho, S.-W.; Lee, S.-Y.; Kang, M.; Lee, B. Synthesis and Dynamic Switching of Surface Plasmon Vortices with Plasmonic Vortex Lens. *Nano Lett.* **2010**, *10*, 529−536.
(27) Schnell, M.; Sarriugarte, P.; Neuman, T.; Khanikaev, A. B.; Shvets, G.; Aizpurua, J.; Hillenbrand, R. Real-Space Mapping of the Chiral Near-Field Distributions in Spiral Antennas and Planar Metasurfaces. *Nano Lett.* **2016**, *16*, 663−670.
(28) Chen, W.; Abeysinghe, D. C.; Nelson, R. L.; Zhan, Q. Experimental Confirmation of Miniature Spiral Plasmonic Lens as a Circular Polarization Analyzer. *Nano Lett.* **2010**, *10*, 2075−2079.
(29) Gorodetski, Y.; Niv, A.; Kleiner, V.; Hasman, E. Observation of the Spin-Based Plasmonic Effect in Nanoscale Structures. *Phys. Rev. Lett.* **2008**, *101*, 043903.
(30) Chen, W.; Abeysinghe, D. C.; Nelson, R. L.; Zhan, Q. Plasmonic Lens Made of Multiple Concentric Metallic Rings under Radially Polarized Illumination. *Nano Lett.* **2009**, *9*, 4320−4325.
(31) Zhao, Y.; Edgar, J. S.; Jeffries, G. D. M.; McGloin, D.; Chiu, D. T. Spin-to-Orbital Angular Momentum Conversion in a Strongly Focused Optical Beam. *Phys. Rev. Lett.* **2007**, *99*, 073901.
(32) Gorodetski, Y.; Shitrit, N.; Bretner, I.; Kleiner, V.; Hasman, E. Observation of Optical Spin Symmetry Breaking in Nanoapertures. *Nano Lett.* **2009**, *9*, 3016−3019.
(33) Li, H.; Zhang, Q.; Yap, C. C. R.; Tay, B. K.; Edwin, T. H. T.; Olivier, A.; Baillargeat, D. From Bulk to Monolayer MoS_2: Evolution of Raman Scattering. *Adv. Funct. Mater.* **2012**, *22*, 1385−1390.
(34) Huang, Y.; Fang, Y.; Zhang, Z.; Zhu, L.; Sun, M. Nanowire-Supported Plasmonic Waveguide for Remote Excitation of Surface-Enhanced Raman Scattering. *Light: Sci. Appl.* **2014**, *3*, e199.
(35) Le, F.; Brandl, D. W.; Urzhumov, Y. A.; Wang, H.; Kundu, J.; Halas, N. J.; Aizpurua, J.; Nordlander, P. Metallic Nanoparticle Arrays: A Common Substrate for Both Surface-Enhanced Raman Scattering and Surface-Enhanced Infrared Absorption. *ACS Nano* **2008**, *2*, 707−718.
(36) Kühn, S.; Håkanson, U.; Rogobete, L.; Sandoghdar, V. Enhancement of Single-Molecule Fluorescence Using a Gold Nanoparticle as an Optical Nanoantenna. *Phys. Rev. Lett.* **2006**, *97*, 017402.
(37) Hannay, J. H. The Majorana Representation of Polarization, and the Berry Phase of Light. *J. Mod. Opt.* **1998**, *45*, 1001−1008.

DOI: 10.1021/acsnano.6b06834
ACS Nano 2017, 11, 1165−1171